Communication

Photoelectric Properties of $GaS_{1-x}Se_x$ ($0 \leq x \leq 1$) Layered Crystals

Yu-Tai Shih [1], Der-Yuh Lin [2,*], Bo-Chang Tseng [3], Ting-Chen Huang [1], Yee-Mou Kao [1], Ming-Cheng Kao [4] and **Sheng-Beng Hwang [5]**

[1] Department of Physics, National Changhua University of Education, Changhua 500207, Taiwan; ytshih@cc.ncue.edu.tw (Y.-T.S.); ymkao@cc.ncue.edu.tw (Y.-M.K.)

[2] Department of Electronic Engineering, National Changhua University of Education, Changhua 500208, Taiwan

[3] Graduate Institute of Photonics, National Changhua University of Education, Changhua 500207, Taiwan

[4] Department of Information and Communication Engineering, Chaoyang University of Technology, Taichung 413310, Taiwan; kmc@cyut.edu.tw

[5] Department of Electronic Engineering, Chienkuo Technology University, Changhua 500020, Taiwan; sbhwa@ctu.edu.tw

* Correspondence: dylin@cc.ncue.edu.tw

Abstract: In this study, the photoelectric properties of a complete series of $GaS_{1-x}Se_x$ ($0 \leq x \leq 1$) layered crystals are investigated. The photoconductivity spectra indicate a decreasing bandgap of $GaS_{1-x}Se_x$ as the Se composition x increases. Time-resolved photocurrent measurements reveal a significant improvement in the response of $GaS_{1-x}Se_x$ to light with increasing x. Frequency-dependent photocurrent measurements demonstrate that both pure GaS crystals and $GaS_{1-x}Se_x$ ternary alloy crystals exhibit a rapid decrease in photocurrents with increasing illumination frequency. Crystals with lower x exhibit a faster decrease in photocurrent. However, pure GaSe crystal maintains its photocurrent significantly even at high frequencies. Measurements for laser-power-dependent photoresponsivity and bias-voltage-dependent photoresponsivity also indicate an increase in the photoresponsivity of $GaS_{1-x}Se_x$ as x increases. Overall, the photoresponsive performance of $GaS_{1-x}Se_x$ is enhanced with increasing x, and pure GaSe exhibits the best performance. This result contradicts the findings of previous reports. Additionally, the inverse trends between bandgap and photoresponsivity with increasing x suggest that $GaS_{1-x}Se_x$-based photodetectors could potentially offer a high response and wavelength-selectivity for UV and visible light detection. Thus, this work provides novel insights into the photoelectric characteristics of $GaS_{1-x}Se_x$ layered crystals and highlights their potential for optoelectronic applications.

Keywords: photoelectric properties; $GaS_{1-x}Se_x$ layered crystals; photoconductivity; Se composition; photocurrent; photoresponsivity

1. Introduction

GaS and GaSe are layered crystals belonging to the IIIA-VIA compound family and are classified as post-transition metal monochalcogenides [1–3]. The room-temperature bandgaps of GaS and GaSe reported in the literature range from 2.46 eV to 2.83 eV [4–10] and 1.95 eV to 2.03 eV [7–14], respectively. Therefore, GaS and GaSe have the potential to be used in the fabrication of optoelectronic devices for applications in the red and blue visible light regions. For instance, GaS has been described as a promising semiconductor for use in near-blue-light-emitting devices [15]. On the other hand, GaSe is also promising for optoelectronic devices in the visible range [16].

GaS and GaSe crystals can be fabricated into atomically thin, two-dimensional (2D) layered structures [17–23] due to the weak van der Waals forces between their adjacent monolayers [1,24]. Recent research has highlighted the intriguing properties exhibited

by these 2D layered structures. For example, the photodetectors based on 2D layered structures of GaSe showed high performance of photoresponse in the UV and visible regions [19,22,25,26]. The GaSe thin film consisting of a few layers displayed a significant absorption coefficient [20]. Furthermore, strong second-harmonic generation was found in atomic layered GaSe [27,28]. On the other hand, the photodetectors based on 2D nanoflakes of GaS demonstrated a relevant UV-selective photoresponse [23]. The superior nonlinear optical activities were also found in the 2D layered structures of GaS [29]. The unique properties and high performance position 2D layered structures of GaS and GaSe as promising materials for applications in next-generation optoelectronics and electronics.

To engineer the properties of GaS and GaSe and expand their potential applications, alloying is one of the crucial methods. For instance, an entire series of $GaS_{1-x}Se_x$ ($0 \leq x \leq 1$) alloy layered crystals can be produced [4,8,9,30–37]. By adjusting the composition ratio of S and Se, the lattice constants [9,30,32,33] and bandgap [8,9,36,37] can be tuned. The ability to tune the bandgap is essential for achieving high-performance optoelectronic devices. Numerous experimental and theoretical studies on $GaS_{1-x}Se_x$ alloy crystals have been conducted [9,37–44], dating back to early reports on the photoconductivity of these alloys in 1960 [8]. For instance, the investigation on the nanobelts of $GaS_{1-x}Se_x$ crystals showed they exhibited an intense photoluminescence spectrum in the visible range for all compositions [37]. More recently, $GaS_{1-x}Se_x$ alloy crystals have been employed as color converters for GaN-based micro light-emitting diodes, enabling the conversion of blue emission to green and red [39]. The exploration of $GaS_{1-x}Se_x$ alloy crystals for electronic and optoelectronic devices has garnered attention, yet comprehensive investigations into their photoelectric characteristics remain limited. Therefore, our study delves into the photoelectric properties of $GaS_{1-x}Se_x$ alloy crystals, aiming to uncover their potential applications. Our experimental results reveal an enhancement in the photoresponsive performance of $GaS_{1-x}Se_x$ with increasing x, with pure GaSe exhibiting the best performance. This finding contradicts previous observations on $GaS_{1-x}Se_x$ nanobelts [37] and $MoS_{2(1-x)}Se_{2x}$ monolayers [45], where a decrease in photocurrents was noted with increasing Se composition x. Additionally, the inverse trends between the bandgap and photoresponsivity with increasing x suggests that the $GaS_{1-x}Se_x$-based photodetectors could potentially offer high response and specific wavelength-selectivity for UV and visible-light-detection applications by adjusting their composition and thickness. Thus, this work introduces novel insights and contributes to assessing the potential of $GaS_{1-x}Se_x$ layered crystals for optoelectronic applications.

2. Materials and Methods

An entire series of $GaS_{1-x}Se_x$ ($0 \leq x \leq 1$) layered crystals was grown using the chemical vapor transportation method with I_2 as a transport agent. High-purity elemental S powder, Ga granules, Se granules, and I_2 pieces were carefully weighed and placed in a quartz ampoule. The ampoule was then evacuated to 10^{-6} torr, sealed, and positioned in a three-zone furnace. To grow pure GaS crystals, the temperatures of the first, second, and third zones of the furnace were set to 950 °C, 900 °C, and 850 °C, respectively. For subsequent growths of $GaS_{1-x}Se_x$ mixed crystals, the molar ratio $x = Se/(S + Se)$ was incrementally increased by 0.2, accompanied by a corresponding reduction of 50 °C in the growth temperatures. Therefore, for the growth of pure GaSe crystals, the temperatures of the furnace's first, second, and third zones were adjusted to 700 °C, 650 °C, and 600 °C, respectively. The crystal growth process typically lasted for approximately 265 h.

The scanning and transmission electron microscopy images of the grown $GaS_{1-x}Se_x$ specimens revealed layered crystals with hexagonal structures and high crystalline quality. Raman and X-ray diffraction analyses indicated that GaS and $GaS_{0.8}Se_{0.2}$ were in the 2H β-phase, GaSe was in the 2H ε-phase, while those with intermediate x were in the 2H β-ε mixed phase. The wavelength of the samples' photoluminescence peaks increased with x and covered the visible range. Detailed information regarding their growth conditions,

composition ratios, structural properties, and optical properties has been previously reported [9]. This study focuses on investigating and reporting their photoelectric properties.

For the absorption and photoconductivity (PC) measurements, a 0.25 m monochromator (MKS, Irvine, CA, USA) equipped with a 130 W halogen lamp was employed to generate monochromatic light across a wide photon energy range. The continuous light from the monochromator was modulated into alternating light using a rotating beam chopper with a frequency set at 200 Hz, which then illuminated the measured sample. For the absorption measurements, a silicon photodetector (Thorlabs, Newton, NJ, USA) with a sensing range of 1.5 to 3.1 eV was positioned at the back of the measured sample. The output signals from the photodetector were captured using an EG&G 7265 Dual Phase DSP Lock-in Amplifier (Test Equipment Solutions, Bedfordshire, UK) to suppress noise signals effectively.

For the PC measurements, the sample under examination was affixed to a copper holder using thin tape. A stable bias voltage of 50 V was applied to the sample using a Keithley 2400 SourceMeter (Tektronix, Beaverton, OR, USA). The low power of the illuminating light, the exceptionally thin adhesive tape, and the efficient heat dissipation of the copper holder ensured minimal temperature rise in the sample during light exposure. This guaranteed that the current observed in the PC experiments stemmed from photoinduction rather than thermal induction. The signals of the induced photocurrent were received and transformed into voltage signals through an SR570 low-noise current preamplifier (Stanford Research Systems, Sunnyvale, CA, USA). An EG&G 7265 Dual Phase DSP Lock-in Amplifier processed the voltage signals, transferring them to a computer via a general-purpose interface bus (GPIB). The photoresponsivity of a measured sample was defined as the induced photocurrent divided by the power of the incident light. The variation in photoresponsivity with the photon energy of the incident light for a specimen was depicted as its PC spectrum.

To measure the photocurrent of a specimen as a function of time or the frequency of alternating illumination, a laser with a wavelength of 405 nm was employed as the excitation source. This laser, controlled by an AFG-2225 function generator (GW Instek, New Taipei City, Taiwan), applied on/off light modulation to the measured specimen. A stable bias voltage of 50 V was applied to the sample using a Keithley 2400 SourceMeter. An SR570 low-noise current preamplifier received the signals of the induced photocurrent and transformed them into voltage signals. For the time-dependent photocurrent measurements, a data acquisition device with a time resolution of 1 μs was employed to collect and transfer these signals to a computer for depicting the variation of photocurrent over time for the measured specimen. For the frequency-dependent photocurrent measurements, an EG&G 7265 Dual Phase DSP Lock-in Amplifier was used to receive the voltage signals and transfer them to a computer via a GPIB. The amplitude of the alternating photocurrent during alternating illumination, I_{ac}, was divided by the steady-state photocurrent during steady illumination, I_{dc}, to obtain the normalized photocurrent I_{ac}/I_{dc} as a function of the frequency of alternating illumination.

To measure the photoresponsivity of a specimen as a function of the incident laser power or the bias voltage, a laser with a wavelength of 405 nm was employed as the excitation source. An AFG-2225 function generator was utilized to modulate the laser light into alternating light with a frequency of 1 Hz. For the bias-dependent photoresponsivity measurements, the laser power was set to 11.6 mW, and a Keithley 2400 SourceMeter was used to apply a bias voltage to the measured sample and record the induced current. The difference between the average currents under illumination and in the dark was divided by the incident laser power to obtain the photoresponsivity of the measured sample. For the laser-power-dependent photoresponsivity measurements, the incident laser power was adjusted using neutral-density filters. A stable bias voltage of 50 V was applied to the measured sample using a Keithley 2400 SourceMeter. The photocurrent was recorded using an EG&G 7265 Dual Phase DSP Lock-in Amplifier and then divided by the incident laser power to obtain the photoresponsivity of the measured sample.

3. Results and Discussion

The room-temperature absorption spectra of the $GaS_{1-x}Se_x$ ($0 \leq x \leq 1$) samples are depicted in Figure 1a. Based on these absorption spectra, we employed the Tauc plot method [46,47] to ascertain the indirect and direct bandgaps of the $GaS_{1-x}Se_x$ samples by extrapolating the linear segment of the $(AE_{ph})^n$ vs. E_{ph} curves at $(AE_{ph})^n = 0$ for $n = 1/2$ and 2, respectively. Here, A represents the absorbance of the measured sample, and E_{ph} signifies the energy of the incident photon. The determined indirect bandgaps of GaS, $GaS_{0.80}Se_{0.20}$, $GaS_{0.60}Se_{0.40}$, $GaS_{0.37}Se_{0.63}$, $GaS_{0.19}Se_{0.81}$, and GaSe are 2.58 eV, 2.45 eV, 2.34 eV, 2.24 eV, 2.16 eV, and 2.00 eV, respectively. Similarly, the determined direct bandgaps of GaS, $GaS_{0.80}Se_{0.20}$, $GaS_{0.60}Se_{0.40}$, $GaS_{0.37}Se_{0.63}$, $GaS_{0.19}Se_{0.81}$, and GaSe are 2.64 eV, 2.49 eV, 2.36 eV, 2.28 eV, 2.18 eV, and 2.02 eV, respectively [9]. It is noted that, as x increases, the sample exhibits a smaller bandgap.
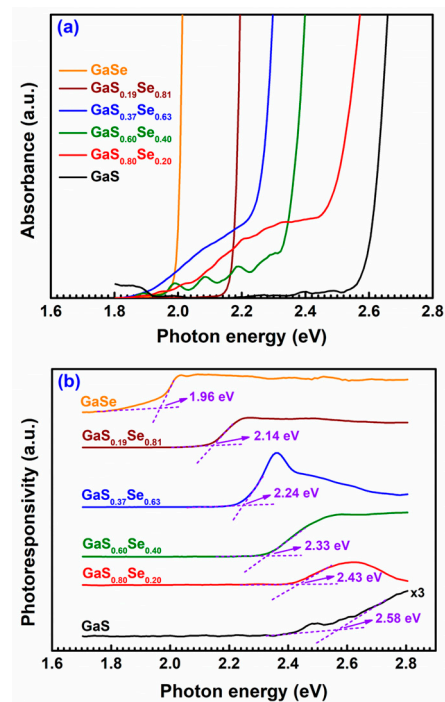

Figure 1. Absorption (**a**) and photoconductivity (**b**) spectra of the $GaS_{1-x}Se_x$ specimens at room temperature.

The room-temperature PC spectra of the $GaS_{1-x}Se_x$ ($0 \leq x \leq 1$) samples are illustrated in Figure 1b. It is apparent that the photoconductivity of each specimen undergoes negligible variations with increasing photon energy until it experiences a sudden increase beyond a specific value. This specific value roughly indicates the bandgap of the specimen. When the photon energy surpasses the bandgap of the semiconductor material, electrons can absorb photons and transition from the valence band to the conduction band, resulting in an increase in the total number of conduction carriers and subsequently enhancing the material's conductivity. The bandgaps of GaS, $GaS_{0.80}Se_{0.20}$, $GaS_{0.60}Se_{0.40}$, $GaS_{0.37}Se_{0.63}$, $GaS_{0.19}Se_{0.81}$, and GaSe are approximately 2.58 eV, 2.43 eV, 2.33 eV, 2.24 eV, 2.14 eV, and 1.96 eV, respectively. The bandgaps determined from the PC spectra of the $GaS_{1-x}Se_x$ samples align with those indirect bandgaps obtained from their absorption spectra.

Figure 2a presents the photocurrent profile of the $GaS_{0.60}Se_{0.40}$ specimen under an illumination frequency of 200 Hz, depicting its variation over time. Similar behaviors were observed for the photocurrents of other $GaS_{1-x}Se_x$ specimens under different illumination frequencies. Figure 2b illustrates the rise times t_{rise}, defined from 10% to 90% of the maximum photocurrent, and the fall times t_{fall}, defined from 90% to 10% of the maximum photocurrent, for the $GaS_{1-x}Se_x$ samples under various illumination frequencies

as functions of the Se composition x. Across all illumination frequencies, t_{rise} and t_{fall} decrease with an increase in the Se composition x. The GaSe sample exhibits the shortest t_{rise} and t_{fall}.
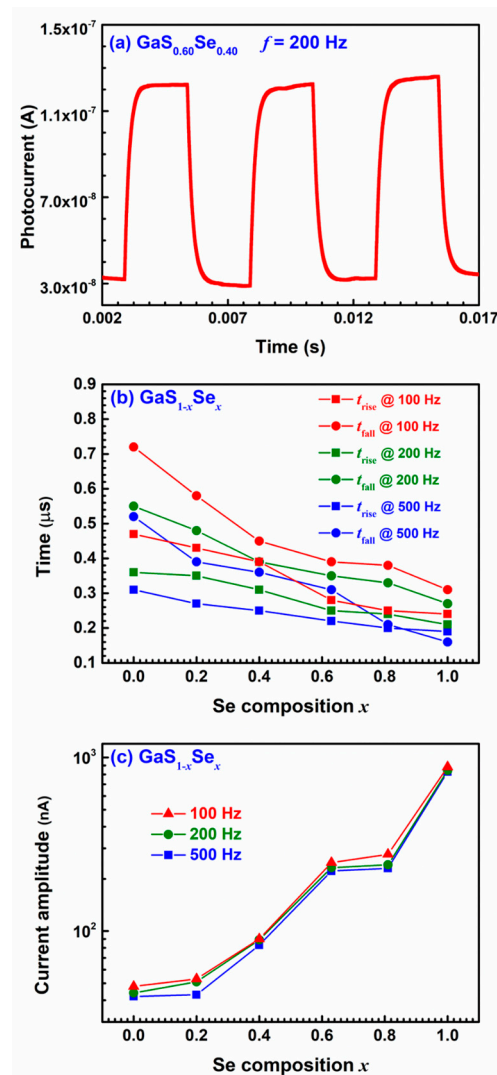

Figure 2. (**a**) Photocurrent of the $GaS_{0.60}Se_{0.40}$ specimen under an illumination frequency of 200 Hz as a function of time. Rise times t_{rise} and fall times t_{fall} (**b**) and current amplitudes (**c**) of the $GaS_{1-x}Se_x$ specimens under variant frequencies of alternating illumination as functions of the Se composition x.

In Figure 2c, the current amplitudes, representing the difference between the maximum and minimum photocurrents in a rising–falling period, are shown for the $GaS_{1-x}Se_x$ samples under different illumination frequencies. Regardless of the illumination frequency, the current amplitude rises with an increase in the Se composition x. The pure GaSe sample attains the highest current amplitude, significantly surpassing those of the $GaS_{1-x}Se_x$ ternary alloy samples and the pure GaS sample. This finding contrasts with previous investigations on both $GaS_{1-x}Se_x$ nanobelts [37] and $MoS_{2(1-x)}Se_{2x}$ monolayers [45], which indicated a decrease in photocurrent as the Se composition x increased. Our result demonstrates the opposite trend.

Figure 3 illustrates the normalized photocurrents I_{ac}/I_{dc} of the $GaS_{1-x}Se_x$ specimens as functions of the frequency f of alternating illumination. For frequencies $f \geq 100$ Hz, a higher Se composition x corresponds to a greater I_{ac}/I_{dc}. The normalized photocurrents decrease rapidly with increasing f for the pure GaS sample and the $GaS_{1-x}Se_x$ ternary alloy samples, with the photocurrent dropping more quickly for samples with lower x. For

frequencies above 1000 Hz, the I_{ac}/I_{dc} for these samples are less than 0.01. In contrast, the normalized photocurrent for GaSe remains significantly high even at high frequencies, exceeding 0.01 at $f = 9000$ Hz, with an I_{ac}/I_{dc} greater than 0.015. Consequently, at high frequencies of alternating illumination, the optical response of the pure GaSe sample surpasses that of both the pure GaS sample and the $GaS_{1-x}Se_x$ ternary alloy samples.
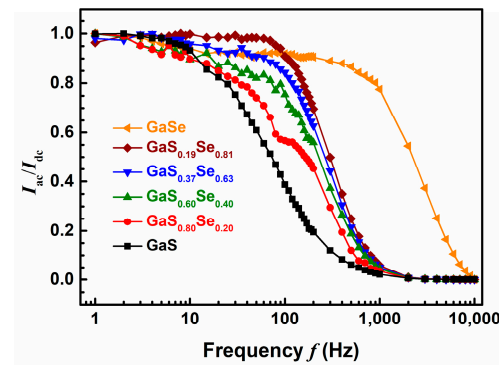
Figure 3. Normalized photocurrents of the $GaS_{1-x}Se_x$ specimens as functions of the frequency of alternating illumination.

Figure 4 illustrates the photoresponsivities of the $GaS_{1-x}Se_x$ specimens as functions of the incident laser power. As the incident laser power gradually decreases from the order of 10^{-2} W to the order of 10^{-6} W, the photoresponsivities of all $GaS_{1-x}Se_x$ samples gradually increase. The GaSe sample exhibits the largest increase, with its photoresponsivity increasing by 85.7 times. For a given incident laser power, the photoresponsivity increases as x increases. The pure GaSe sample possesses the highest photoresponsivity at any laser power, exceeding that of other samples by at least one order of magnitude. The maximum photoresponsivity of the pure GaSe sample reaches 5.77×10^{-3} A/W at a laser power of 8.70×10^{-7} W, significantly greater than those of the $GaS_{1-x}Se_x$ ternary alloy samples and the pure GaS sample. Conversely, the pure GaS sample has the lowest maximum photoresponsivity at a laser power of 8.70×10^{-7} W, which is 1.78×10^{-6} A/W.
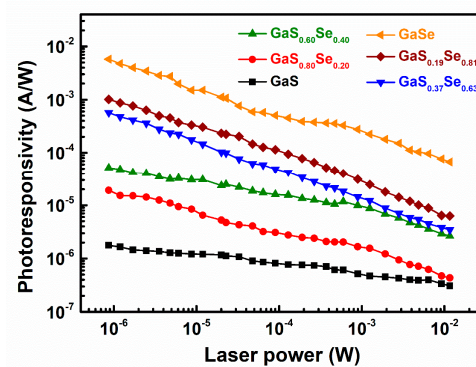
Figure 4. Photoresponsivities of the $GaS_{1-x}Se_x$ specimens as functions of the incident laser power.

Figure 5 illustrates how the photoresponsivities of the $GaS_{1-x}Se_x$ samples vary with the bias voltage. As the applied bias voltage increases from 5 V to 50 V, the photoresponsivities of all $GaS_{1-x}Se_x$ samples gradually increase. For a given bias voltage, the photoresponsivity increases as x increases. The pure GaSe sample exhibits the highest photoresponsivity at any bias voltage, exceeding that of other samples by at least one order of magnitude. At a bias voltage of 5 V, the photoresponsivities of the $GaS_{1-x}Se_x$ samples increase from 8.44×10^{-9} A/W to 3.76×10^{-6} A/W as x increases from 0 to 1. This contrasts with the findings of Jung et al. [37], who reported that the photoresponsivities of $GaS_{1-x}Se_x$ nanobelts at 2 V were approximately 7×10^{-6} A/W for x ranging from 0 to 0.5, decreasing

to approximately 1×10^{-6} A/W for $x = 0.7$ and approximately 0.5×10^{-6} A/W for $x = 1$. Our measured photoresponsivity changes with x in the opposite direction of theirs. The photoresponsivity of our pure GaSe sample reaches its maximum value of 6.39×10^{-5} A/W at 50 V, significantly greater than those of the $GaS_{1-x}Se_x$ ternary alloy samples and the pure GaS sample. Conversely, the pure GaS sample has the lowest maximum photoresponsivity at a bias voltage of 50 V, which is 3.34×10^{-7} A/W.
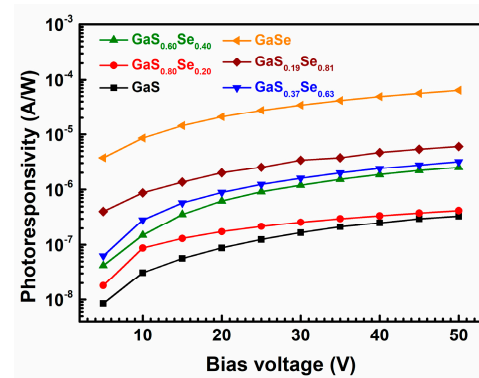
Figure 5. Photoresponsivities of the $GaS_{1-x}Se_x$ specimens as functions of the bias voltage.

Ho et al. investigated the photoconductance and photoresponse of the photodetectors based on $GaS_{1-x}Se_x$ layered crystals, ranking the photosensitivity of their samples from maximum to minimum as $GaS_{0.3}Se_{0.7}$, $GaS_{0.2}Se_{0.8}$, $GaS_{0.4}Se_{0.6}$, $GaS_{0.1}Se_{0.9}$, GaSe, and GaS [48]. However, our results, as discussed above, differ from those of Ho et al. [48]. We found that the photoresponsive performance of the $GaS_{1-x}Se_x$ samples improves monotonously with increasing x, with the pure GaSe sample exhibiting the best performance.

The enhancement in photoresponsive performance may be attributed to the decreased bandgaps of the $GaS_{1-x}Se_x$ samples with increasing x. The redshift of the bandgaps occurs because an increase in the Se composition x results in more S ions being replaced by Se ions, leading to an increase in lattice constants and, consequently, a decrease in bandgaps. A smaller bandgap facilitates the transition of an electron from the valence band to the conduction band by absorbing a photon. The increased number of carriers generated by the absorption of photons enhances the photoresponsive performance of the semiconductors.

Another factor contributing to enhancing the photoresponsive performance of $GaS_{1-x}Se_x$ layered crystals may be the reduction in the difference between indirect and direct bandgaps as x increases. The minimum difference is only 20 meV when $x = 1$. This insignificant energy difference makes the $GaS_{1-x}Se_x$ crystals with high x resemble pseudo-direct bandgap semiconductors [9]. Semiconductors with direct bandgaps exhibit better response to light. Consequently, the photoresponsive performance of the $GaS_{1-x}Se_x$ crystals is enhanced with increasing x.

It is well known that GaX (X = S or Se) layered crystals exhibit four basic polytypes determined by the stacking sequences of the monolayers: 2H β-, 2H ε-, 3R γ-, and 4H δ-GaX, corresponding to the space groups $P6_3/mmc$ (D_{6h}^4), $P\bar{6}m2$(D_{3h}^1), $R3m$ (C_{3v}^5), and $P6_3mc$ (C_{6v}^4) [9]. These distinct stacking arrangements give rise to variations in the properties of GaX crystals across different phases. Building upon this understanding, we propose another intriguing hypothesis suggesting that the photoresponsive performance of $GaS_{1-x}Se_x$ layered crystals may be influenced by their polytypes. Jung et al. [37] demonstrated that their pure GaS existed in the β phase, while the $GaS_{1-x}Se_x$ ternary alloys and pure GaSe were in a β-γ mixed phase. With increasing x, the ratio of β to γ phases decreased. Conversely, our pure GaS and $GaS_{0.80}Se_{0.20}$ ternary alloy were in the β-phase. $GaS_{0.60}Se_{0.40}$, $GaS_{0.37}Se_{0.63}$, and $GaS_{0.19}Se_{0.81}$ ternary alloys exhibited a β-ε mixed phase, with the ratio of β to ε phases decreasing with increasing x. Pure GaSe was in the ε phase. If we hypothesize that the ε and γ phases have the best and worst photoresponsive performance, respectively, with the β phase exhibiting intermediate performance, it may explain the

contrast between our findings and those of Jung et al. [37], who reported a decrease in the photoresponsive performance of $GaS_{1-x}Se_x$ nanobelts with increasing x. However, growing $GaS_{1-x}Se_x$ crystals exclusively in one pure phase for all different phases remains challenging. Therefore, confirming this hypothesis would require the development of a state-of-the-art growth technique for $GaS_{1-x}Se_x$ crystals, presenting an intriguing task for future research.

The bandgaps of $GaS_{1-x}Se_x$ layered crystals span the visible region, but they can significantly increase to over 3.0 eV and extend into the UV region when reduced to the monolayer state due to the quantum confinement effect [36,49]. Photodetectors based on 2D nanoflakes of GaS have shown a remarkable UV-selective photoresponse attributed to the increased bandgaps [23,50,51]. Considering the photoelectric properties of $GaS_{1-x}Se_x$ layered crystals, the decrease in bandgaps with increasing x implies that $GaS_{1-x}Se_x$ crystals with $x > 0$ respond to longer wavelengths compared to pure GaS crystals. Additionally, the enhancement of photoresponsive performance with increasing x suggests that $GaS_{1-x}Se_x$ crystals with $x > 0$ exhibit higher photoresponsivity than pure GaS crystals. Consequently, $GaS_{1-x}Se_x$-based photodetectors could potentially offer high response and specific wavelength-selectivity for UV and visible-light-detection applications by adjusting their composition and thickness, thereby broadening the potential applications of $GaS_{1-x}Se_x$ layered crystals in optoelectronics.

4. Conclusions

The photoelectric properties of a complete series of $GaS_{1-x}Se_x$ ($0 \leq x \leq 1$) layered crystals were investigated. The photoconductivity spectra revealed that the bandgap of $GaS_{1-x}Se_x$ gradually decreases as the Se composition x increases. The time-dependent photocurrent measurements demonstrated that the increase in x significantly improves the response of $GaS_{1-x}Se_x$ to light. The pure GaSe crystal has the shortest rise and fall times and the largest current amplitude. The frequency-dependent photocurrent measurements indicated that the photocurrents of the pure GaS crystal and $GaS_{1-x}Se_x$ ternary alloy crystals decrease rapidly as the frequency of alternating illumination increases. Crystals with lower x have a faster decrease in photocurrent. However, the photocurrent of the pure GaSe crystal persists significantly, even at high frequencies. Additionally, the measurements for laser-power-dependent photoresponsivity and bias-voltage-dependent photoresponsivity revealed that the increase in x enhances the photoresponsivity of $GaS_{1-x}Se_x$. Overall, the photoresponsive performance of $GaS_{1-x}Se_x$ improves with increasing x, with pure GaSe exhibiting the best performance. This result contradicts the findings of the previous report. This enhancement in photoresponsive performance of the $GaS_{1-x}Se_x$ layered crystals may be attributed to several factors, including decreasing bandgaps, reduced differences between indirect and direct bandgaps, and phase conversion from β-GaS to ε-GaSe as x increases. Because the bandgap and the photoresponsivity of $GaS_{1-x}Se_x$ vary in reverse trends as x increases, the $GaS_{1-x}Se_x$-based photodetectors could potentially offer high response and specific wavelength-selectivity for UV- and visible-light-detection applications by adjusting their composition and thickness. The findings of this work provide novel insights into the photoelectric characteristics of $GaS_{1-x}Se_x$ layered crystals and contribute to assessing the viability of $GaS_{1-x}Se_x$ layered crystals for potential use in optoelectronics.

References

1. Terhell, J.C.J.M. Polytypism in the III–VI layer compounds. *Prog. Cryst. Growth Charact.* **1983**, *7*, 55–110. [CrossRef]
2. Cai, H.; Gu, Y.; Lin, Y.-C.; Yu, Y.; Geohegan, D.B.; Xiao, K. Synthesis and emerging properties of 2D layered III–VI metal chalcogenides. *Appl. Phys. Rev.* **2019**, *6*, 041312. [CrossRef]
3. Arora, H.; Erbe, A. Recent progress in contact, mobility, and encapsulation engineering of InSe and GaSe. *InfoMat.* **2021**, *3*, 662–693. [CrossRef]
4. Ho, C.H.; Huang, K.W. Visible luminescence and structural property of $GaSe_{1-x}S_x$ ($0 \leq x \leq 1$) series layered crystals. *Solid State Comm.* **2005**, *136*, 591–594. [CrossRef]
5. Ho, C.H.; Lin, S.L. Optical properties of the interband transitions of layered gallium sulfide. *J. Appl. Phys.* **2006**, *100*, 083508. [CrossRef]
6. Kępińska, M.; Nowak, M.; Szalajko, M. Temperature dependence of optical parameters of gallium sulphide. *J. Wide Bandgap Mater.* **2001**, *8*, 241–249. [CrossRef]
7. Isik, M.; Gasanly, N. Composition-tuned band gap energy and refractive index in GaS_xSe_{1-x} layered mixed crystals. *Mater. Chem. Phys.* **2017**, *190*, 74–78. [CrossRef]
8. Bube, R.H.; Lind, E.L. Photoconductivity in gallium sulfo-selenide solid solutions. *Phys. Rev.* **1960**, *119*, 1535–1537. [CrossRef]
9. Shih, Y.-T.; Lin, D.-Y.; Tseng, B.-C.; Kao, Y.-M.; Hwang, S.-B.; Lin, C.-F. Structural and optical characterization of $GaS_{1-x}Se_x$ layered mixed crystals grown by chemical vapor transport. *Mater. Today Comm.* **2023**, *37*, 107047. [CrossRef]
10. Nizametdinpova, Y.A. The refleotion spectrum of GaSe and Gas single crystals near the fundamental absorption edge. *Phys. Stat. Sol.* **1967**, *19*, k111–k112.
11. Fernelius, N.C. Properties of gallium Selenide single crystal. *Prog. Cryst. Growth Charact.* **1994**, *28*, 275–353. [CrossRef]
12. Bube, R.H.; Lind, E.L. Photoconductivity of gallium selenide crystals. *Phys. Rev.* **1959**, *115*, 1159–1164. [CrossRef]
13. Wu, C.C.; Ho, C.H.; Shen, W.T.; Cheng, Z.H.; Huang, Y.S.; Tiong, K.K. Optical properties of $GaSe_{1-x}S_x$ series layered semiconductors grown by vertical Bridgman method. *Mater. Chem. Phys.* **2004**, *88*, 313–317. [CrossRef]
14. Madelung, O. *Semiconductors: Data Handbook*, 3rd ed.; Springer: Marburg, Germany, 2004; p. 515.
15. Aono, T.; Kase, K.; Kinoshita, A. Near-blue photoluminescence of Zn-doped GaS single crystals. *J. Appl. Phys.* **1993**, *74*, 2818–2820. [CrossRef]
16. Shigetomi, S.; Ikari, T.; Nakashima, H. Impurity levels in layer semiconductor *p*-GaSe doped with Mn. *J. Appl. Phys.* **1994**, *76*, 310–314. [CrossRef]
17. Chen, M.-W.; Kim, H.; Ovchinnikov, D.; Kuc, A.; Heine, T.; Renault, O.; Kis, A. Large-grain MBE-grown GaSe on GaAs with a Mexican hatlike valence band dispersion. *NPJ 2D Mater.* **2018**, *2*, 2. [CrossRef]
18. Afaneh, T.; Fryer, A.; Xin, Y.; Hyde, R.H.; Kapuruge, N.; Gutiérrez, H.R. Large-area growth and stability of monolayer gallium monochalcogenides for optoelectronic devices. *ACS Appl. Nano Mater.* **2020**, *3*, 7879–7887. [CrossRef]
19. Hu, P.; Wen, Z.; Wang, L.; Tan, P.; Xiao, K. Synthesis of few-layer GaSe nanosheets for high performance photodetectors. *ACS Nano* **2012**, *6*, 5988–5994. [CrossRef] [PubMed]
20. Bassou, A.; Rajira, A.; El-Hattab, M.; Haskouri, J.E.; Murcia-Mascaros, S.; Almaggoussi, A.; Abounadi, A. Structural and optical properties of a layered ε-GaSe thin film under elastic deformation from flexible PET substrate. *Micro Nanostruct.* **2022**, *163*, 107152. [CrossRef]
21. Gutiérrez, Y.; Giangregorio, M.M.; Dicorato, S.; Palumbo, F.; Losurdo, M. Exploring the thickness-dependence of the properties of layered gallium sulfide. *Front. Chem.* **2021**, *9*, 781467. [CrossRef]
22. Curreli, N.; Serri, M.; Zappia, M.I.; Spirito, D.; Bianca, G.; Buha, J.; Najafi, L.; Sofer, Z.; Krahne, R.; Pellegrini, V.; et al. Liquid-phase exfoliated gallium selenide for light-driven thin-film transistors. *Adv. Electron. Mater.* **2021**, *7*, 2001080. [CrossRef]
23. Zappia, M.I.; Bianca, G.; Bellani, S.; Curreli, N.; Sofer, Z.; Serri, M.; Najafi, L.; Piccinni, M.; Oropesa-Nunez, R.; Marvan, P.; et al. Two-dimensional gallium sulfide nanoflakes for UV-selective photoelectrochemical-type photodetectors. *J. Phys. Chem. C* **2021**, *125*, 11857–11866. [CrossRef] [PubMed]
24. Scrocco, M. Electron-energy-loss spectra of GaSe and Ga metal. *Phys. Rev. B* **1987**, *36*, 9732–9735. [CrossRef] [PubMed]
25. Lei, S.; Ge, L.; Liu, Z.; Najmaei, S.; Shi, G.; You, G.; Lou, J.; Vajtai, R.; Ajayan, P.M. Synthesis and photoresponse of large GaSe atomic layers. *Nano Lett.* **2013**, *13*, 2777–2781. [CrossRef] [PubMed]
26. Cao, Y.; Cai, K.; Hu, P.; Zhao, L.; Yan, T.; Luo, W.; Zhang, X.; Wu, X.; Wang, K.; Zheng, H. Strong enhancement of photoresponsivity with shrinking the electrodes spacing in few layer GaSe photodetectors. *Sci. Rep.* **2015**, *5*, 8130. [CrossRef]

27. Karvonen, L.; Säynätjoki, A.; Mehravar, S.; Rodriguez, R.D.; Hartmann, S.; Zahn, D.R.T.; Honkanen, S.; Norwood, R.A.; Peyghambarian, N.; Kieu, K.; et al. Investigation of second- and third- harmonic generation in few-layer gallium selenide by multiphoton microscopy. *Sci. Rep.* **2015**, *5*, 10334. [CrossRef] [PubMed]

28. Zhou, X.; Cheng, J.; Zhou, Y.; Cao, T.; Hong, H.; Liao, Z.; Wu, S.; Peng, H.; Liu, K.; Yu, D. Strong second-harmonic generation in atomic layered GaSe. *J. Am. Chem. Soc.* **2015**, *137*, 7994–7997. [CrossRef] [PubMed]

29. Ahmed, S.; Cheng, P.K.; Qiao, J.; Gao, W.; Saleque, A.M.; Ivan, M.N.A.S.; Wang, T.; Alam, T.I.; Hani, S.U.; Guo, Z.L.; et al. Nonlinear optical activities in two-dimensional gallium sulfide: A comprehensive study. *ACS Nano* **2022**, *16*, 12390–12402. [CrossRef] [PubMed]

30. Arancia, G.; Grandolfo, M.; Manfredotti, C.; Rizzo, A. Electron diffraction study of melt- and vapour-grown $GaSe_{1-x}S_x$ single crystals. *Phys. Stat. Sol. (a)* **1976**, *33*, 563–571. [CrossRef]

31. Ho, C.H.; Wu, C.C.; Cheng, Z.H. Crystal structure and electronic structure of $GaSe_{1-x}S_x$ series layered solids. *J. Crystal Grow.* **2005**, *279*, 321–328. [CrossRef]

32. Terhell, J.C.J.M.; Lieth, R.M.A. Preparation and crystallography of gallium sulfide-selenide solid solutions. *Phys. Stat. Sol. (a)* **1971**, *5*, 719–724. [CrossRef]

33. Whitehouse, C.R.; Balchin, A.A. Structural studies of compounds in the series GaS_xSe_{1-x} ($0 \leq x \leq 1$) grown by iodine vapour transport. *J. Mater. Sci.* **1978**, *13*, 2394–2402. [CrossRef]

34. Aulich, E.; Brebner, J.L.; Mooser, E. Indirect energy gap in GaSe and Gas. *Phys. Stat. Sol.* **1969**, *31*, 129–131. [CrossRef]

35. Mercier, A.; Voitchovsky, J.P. Raman scattering from GaS_xSe_{1-x}. *Solid State Comm.* **1974**, *14*, 757–762. [CrossRef]

36. Jung, C.S.; Shojaei, F.; Park, K.; Oh, J.Y.; Im, H.S.; Jang, D.M.; Park, J.; Kang, H.S. Red-to-ultraviolet emission tuning of two-dimensional gallium sulfide/selenide. *ACS Nano* **2015**, *9*, 9585–9593. [CrossRef] [PubMed]

37. Jung, C.S.; Park, K.; Shojaei, F.; Oh, J.Y.; Im, H.S.; Lee, J.A.; Jang, D.M.; Park, J.; Myoung, N.; Lee, C.-L.; et al. Photoluminescence and photocurrents of $GaS_{1-x}Se_x$ Nanobelts. *Chem. Mater.* **2016**, *28*, 5811–5820. [CrossRef]

38. Asadov, S.M.; Mustafaeva, S.N.; Mammadov, A.N. Thermodynamic assessment of phase diagram and concentration–temperature dependences of properties of solid solutions of the GaS–GaSe system. *J. Therm. Anal. Calorim.* **2018**, *133*, 1135–1141. [CrossRef]

39. Tsuboi, Y.; Urakami, N.; Hashimoto, Y. Photoluminescence of layered semiconductor materials for emission-color conversion of blue micro light-emitting diode (μLED). *Coatings* **2020**, *10*, 985. [CrossRef]

40. Huang, C.-B.; Wu, H.-X.; Ni, Y.-B.; Wang, Z.-Y.; Qi, M.; Zhang, C.-L. First-principles calculation of the structural, electronic, elastic, and optical properties of sulfur-doping ε-GaSe crystal. *Chin. Phys. B* **2016**, *25*, 086201. [CrossRef]

41. Zhang, W.X.; Shi, C.H.; He, C. Novel two-dimensional $Ga(In)S_{1-x}Se_x$ as high-efficiency OER catalysts for photocatalytic water splitting. *J. Solid State Chem.* **2020**, *292*, 121730. [CrossRef]

42. Wines, D.; Saritas, K.; Ataca, C. A pathway towards high throughput quantum Monte Carlo simulations for alloys: A case study of two-dimensional (2D) GaS_xSe_{1-x}. *J. Chem. Phys.* **2021**, *155*, 194112. [CrossRef] [PubMed]

43. Ma, T.; Li, Z.; Zhang, H.; Zhu, C.; Lei, Z.; Yang, C. Electronic, optical and lattice dynamics properties of layered $GaSe_{1-x}S_x$. *Mater. Today Comm.* **2021**, *27*, 102212. [CrossRef]

44. Mosaferi, M.; Sarsari, I.A.; Alaei, M. Band structure engineering in gallium sulfide nanostructures. *Appl. Phys. A* **2021**, *127*, 123. [CrossRef]

45. Klee, V.; Preciado, E.; Barroso, D.; Nguyen, A.E.; Lee, C.; Erickson, K.J.; Triplett, M.; Davis, B.; Lu, I.-H.; Bobek, S.; et al. Superlinear composition-dependent photocurrent in CVD-grown monolayer $MoS_{2(1-x)}Se_{2x}$ alloy devices. *Nano Lett.* **2015**, *15*, 2612–2619. [CrossRef] [PubMed]

46. Tauc, J.; Grigorvici, R.; Vancu, A. Optical properties and electronic structure of amorphous germanium. *Phys. Status Solidi* **1966**, *15*, 627–637. [CrossRef]

47. Tauc, J. Optical properties and electronic structure of amorphous Ge and Si. *Mat Res. Mull.* **1968**, *3*, 37–46. [CrossRef]

48. Ho, C.-H.; Hsieh, M.-H.; Wu, C.-C. Photoconductance and photoresponse of layer compound photodetectors in the UV-visible region. *Rev. Sci. Instrum.* **2006**, *77*, 113102. [CrossRef]

49. Zhuang, H.L.; Hennig, R.G. Single-layer group-III monochalcogenide photocatalysts for water splitting. *Chem. Mater.* **2013**, *25*, 3232–3238. [CrossRef]

50. Lu, Y.; Chen, J.; Chen, T.; Shu, Y.; Chang, R.; Sheng, Y.; Shautsova, V.; Mkhize, N.; Holdway, P.; Bhaskaran, H.; et al. Controlling defects in continuous 2D GaS films for high-performance wavelength-tunable UV-discriminating photodetectors. *Adv. Mater.* **2020**, *32*, 1906958. [CrossRef]

51. Hu, P.; Wang, L.; Yoon, M.; Zhang, J.; Feng, W.; Wang, X.; Wen, Z.; Idrobo, J.C.; Miyamoto, Y.; Geohegan, D.B.; et al. Highly responsive ultrathin GaS nanosheet photodetectors on rigid and flexible substrates. *Nano Lett.* **2013**, *13*, 1649–1654. [CrossRef]